Ultrafast Science
A SCIENCE PARTNER JOURNAL

RESEARCH ARTICLE

Probing Interface of Perovskite Oxide Using Surface-Specific Terahertz Spectroscopy

Yudan Su[1,2†], Jiaming Le[1†], Junying Ma[1†], Long Cheng[3], Yuxuan Wei[1], Xiaofang Zhai[3], and Chuanshan Tian[1*]

[1]Department of Physics, State Key Laboratory of Surface Physics and Key Laboratory of Micro- and Nano-Photonic Structure (MOE), Fudan University, Shanghai 200433, China. [2]Department of Physics, University of California, Berkeley, Berkeley, CA 94720, USA. [3]School of Physical Science and Technology, ShanghaiTech University, Shanghai 201210, China.

*Address correspondence to: cstian@fudan.edu.cn
†These authors contributed equally to this work.

Citation: Su Y, Le J, Ma J, Cheng L, Wei Y, Zhai X, Tian C. Probing Interface of Perovskite Oxide Using Surface-Specific Terahertz Spectroscopy. *Ultrafast Sci.* 2023;3:Article 0042. https://doi.org/10.34133/ultrafastscience.0042

Submitted 8 May 2023
Accepted 3 August 2023
Published 18 August 2023

The surface/interface species in perovskite oxides play essential roles in many novel emergent physical phenomena and chemical processes. With low eigen-energies in the terahertz region, such species at buried interfaces remain poorly understood due to the lack of feasible surface-specific spectroscopic probes to resolve the resonances. Here, we show that polarized phonons and two-dimensional electron gas at the interface can be characterized using surface-specific nonlinear optical spectroscopy in the terahertz range. This technique uses intra-pulse difference frequency mixing process, which is allowed only at the surface/interface of a centrosymmetric medium. Submonolayer sensitivity can be achieved using the state-of-the-art detection scheme for the terahertz emission from the surface/interface. Through symmetry analysis and proper polarization selection, background-free Drude-like nonlinear response from the two-dimensional electron gas emerging at the $LaAlO_3/SrTiO_3$ or $Al_2O_3/SrTiO_3$ interface was successfully observed. The surface/interface potential, which is a key parameter for $SrTiO_3$-based interface superconductivity and photocatalysis, can now be determined optically in a nonvacuum environment via quantitative analysis on the phonon spectrum that was polarized by the surface field in the interfacial region. The interfacial species with resonant frequencies in the THz region revealed by our method provide more insights into the understanding of physical properties of complex oxides.

Introduction

The surface and interface of complex oxides attract enormous research attention due to their unique electrical, magnetic, and chemical catalytic properties [1,2]. Being a prototypical perovskite oxide, strontium titanate [$SrTiO_3$ (STO)] stands out as an ideal test bed for exploring multifarious intriguing physical and chemical phenomena at heterogeneous interfaces [3], because of its multifunctional nature and the capability of fabrication and modification with atomic-level precision. The collective elementary excitation and coupling present at the surface/interface play a key role in those emergent unique properties [4,5]. For example, at the FeSe/STO interface, it is believed that both low-frequency phonons in STO and interfacial band bending are vital for the enhancement of superconductivity [6,7]. The nontrivial topological vortex/antivortex forming at the interface of $PbTiO_3$/STO, the collective resonance of which lies in the terahertz (THz) range, provides an alternative choice for post-Moore electronic devices [8]. In the case of STO-based photocatalysis, the facet-dependent surface potential is considered as the essential factor for electron-hole separation and charge transfer across the interface, through which water splitting with almost unity quantum efficiency can be realized [9–11]. However, the experimental interrogation of fundamental excitations at surfaces/interfaces in the THz range remains challenging because few surface-specific probes with chemical selectivity are available, especially in hostile environments such as nonvacuum conditions or buried interfaces.

Second-order nonlinear optical spectroscopy, such as sum-frequency spectroscopy (SFS), has been widely employed to study surfaces and interfaces in multidisciplinary areas. Being an all-optical detection scheme, it is the method of choice to probe electronic or vibrational resonances in various complex interfacial systems with submonolayer sensitivity [12]. Unfortunately, for resonant frequency below 15 THz, employing SFS is extremely difficult because of the lack of intense THz light source or a feasible detection scheme that can distinguish the weak sum-frequency signal from the pump light. As a result, over the past decades, applications of surface-specific nonlinear optical spectroscopy have been limited to systems with resonant frequencies ranging from mid-infrared (IR) to ultraviolet. Bear in mind that many important excitations lie in the THz range [13,14], e.g., lattice vibrations, quasi-particles in quantum materials, and hydrogen-bond vibrations in

biomolecules. Thus, the development of surface-specific optical spectroscopic techniques to resolve these surface resonance features in the THz range is desired.

Contrary to the well-established SFS, difference frequency spectroscopy (DFS) was eventually ignored for the study of surface vibrational resonances after a few attempts [15,16] due to the following major difficulties: (a) much lower dipole radiation efficiency of the IR than the visible, (b) lack of highly sensitive detectors for the mid-IR or far-IR photons, and (c) large background noise from fluorescence and black body radiation. However, in the THz range, DFS naturally possesses an obvious advantage over SFS, because DFS does not require an intense IR pump beam, which is unfortunately very difficult to attain below 15 THz. Several studies on the THz emission from the surface of semiconductors or metal have been reported using optical rectification (or, in general, degenerate DF generation) [17–20]. Yet, the resonant features, which are the fingerprints of surface species, were not resolved in those pioneering works. Furthermore, the THz emission observed in those works requires necessarily large nonlinearity of, e.g., the free carriers in metal [17] or photo-carriers in semiconductors [18]. Other recent studies of optical rectification on two-dimensional materials, including monolayer graphene [19] and transition-metal dichalcogenides [20], also need large nonlinear responses owing to strong enhancement through electronic resonances. Thus, it remains unsettled whether optical rectification or DFS is a viable surface-specific tool with chemical selectivity for surface science in general. In this work, using STO as an example, we exploit the potential of DFS as an effective surface-specific analytical remote probe with submonolayer sensitivity for low-frequency excitations at the interface of complex oxides. We expect the THz-DFS to benefit multidisciplinary surface studies, including chiral vibrations of biomolecules and collective motions of hydrogen-bonding networks at interfaces [21,22].

Difference frequency spectroscopy

Being a second-order nonlinear process, DFS is forbidden in the bulk of centrosymmetric medium under electric dipole approximation but is allowed at the surface/interface, where translational continuity is necessarily broken. As for THz-DFS, akin to the formalism of SFS, the field spectrum of generated THz radiation can be expressed as [12]:

$$E_{\mathrm{THz}}(\Omega) \propto \chi^{(2)}_{\mathrm{s,eff}}(\Omega) \int \mathrm{d}\omega \times E(\omega) E^{*}(\omega - \Omega) \tag{1}$$

with

$$\chi^{(2)}_{\mathrm{s,eff}}(\Omega) = \chi^{(2)}_{\mathrm{s}}(\Omega) + \chi^{(3)}_{\mathrm{B}}(\Omega) \int E_0(z) e^{i\Delta k z} \mathrm{d}z \tag{2}$$

and $E(\omega)$ is the spectrum of the pump field. Here, the effective second-order surface nonlinear susceptibility, $\chi^{(2)}_{\mathrm{s,eff}}$, contains both $\chi^{(2)}_{\mathrm{s}}$ from the surface structure and $\chi^{(3)}_{\mathrm{B}} \int E_0(z) e^{i\Delta k z} \mathrm{d}z$ from surface field-induced polarization in the depletion layer, with $\chi^{(3)}_{\mathrm{B}}$ being the third-order nonlinear susceptibility of the bulk and $E_0(z)$ being the depth-dependent static surface field [23]. Δk is the phase mismatch along surface normal. In the case that the coherence length $l_c = 1/\Delta k$ is much larger than the thickness of the depletion layer, the second term on the right hand side of Eq. 2 reduces to

$$\chi^{(3)}_{\mathrm{B}}(\Omega) \int E_0(z) e^{i\Delta k z} \mathrm{d}z \cong \chi^{(3)}_{\mathrm{B}} \int E_0(z) \mathrm{d}z = \chi^{(3)}_{\mathrm{B}} \Phi \tag{3}$$

where Φ is the surface potential [24]. Thus, $\chi^{(2)}_{\mathrm{s,eff}}$ can be used to characterize both the surface structure and the surface potential, Φ. In the study of a buried interface or multilayer materials, the main advantage of THz-DFS over second harmonic spectroscopy is that the former probes a selected side of the target interface with chemical sensitivity, while the latter contains contributions from all interfaces [25].

In the experiment, the THz radiation is generated via intra-pulse DFS of a femtosecond pump pulse from a surface/interface (Fig. 1A and B). In contrast to conventional difference frequency mixing (DFM) process, in which typically two input beams are involved, the intra-pulse DFM uses the frequency components within the spectral range of the pump pulse. Thus, in measurement, only a single ultrashort pulse with a broad bandwidth is required to pump the sample. Generally, the magnitude of $\chi^{(2)}_{\mathrm{s}}$ for a surface/interface is in the range of 10^{-20} to 10^{-22} $\mathrm{m^2/V}$. Using 1 $\mathrm{TW/cm^2}$ pump intensity, the field strength of the THz output is estimated to be in the order of 10^{0} to 10^{-2} V/cm. Such a weak THz radiation can be measured using the state-of-the-art electro-optic sampling (EOS) technique. EOS measures THz field, $E_{\mathrm{THz}}(t)$, transients coherently in the time domain but largely suppresses thermal or fluorescence background. Then, the spectrum of THz field, $E_{\mathrm{THz}}(\Omega)$, can be obtained from the Fourier transformation of $E_{\mathrm{THz}}(t)$. Recently, we managed to improve the detection in our EOS to a sensitivity [26] of 5×10^{-8} rad $\mathrm{Hz^{-1/2}}$ for 100-kHz femtosecond laser system, which corresponds to the detection sensitivity of $\chi^{(2)}_{\mathrm{s}}$ reaching 2×10^{-21} $\mathrm{m^2\ V^{-1}\ Hz^{-1/2}}$ (see Methods). It is sufficient to probe submonolayer thick interfacial species with $\chi^{(2)}_{\mathrm{s}} \sim 2 \times 10^{-22}$ $\mathrm{m^2/V}$ with an acquisition time of 100 s. The sketch in Fig. 1D shows the key components of the THz-DFS measurement apparatus (see Methods for details).

Methods

Experimental setup

The experimental setup of THz-DFS is shown schematically in Fig. 1D. The system is based on a Yb:KGW regenerative amplifier (Light Conversion PHAROS) operating at 100-kHz repetition rate. The amplifier output centered at 1,030 nm undergoes a nonlinear spectral broadening stage as described elsewhere [27]. After reflecting on a set of chirped mirrors, the pulse was compressed to 26 fs. A tiny portion was picked out by a beam splitter to be used as the probe pulse in EOS, while the majority pumps the intra-pulse difference frequency generation (DFG) process on the sample surface/interface. The incident pump was 44 μJ in energy per pulse and is focused to 0.5 mm ($1/e^2$ diameter) on the sample. An achromatic half wave plate is used to rotate the pump polarization. The emitted THz pulse in the reflecting direction was collimated and refocused onto a 0.3-mm-thick GaP(110) crystal by a pair of parabolic mirrors with 200- and 100-mm focal length, respectively. Between the two parabolic mirrors, a broadband wire grid polarizer was used as the analyzer for the THz radiation. The reflected residual pump was filtered out by a Teflon plate. The whole THz beam path was purged with dry air to avoid vapor absorption. The probe beam was combined collinearly with THz beam by a Ge wafer. The relative delay between the THz beam and probe pulse was controlled by a delay line stage shown in Fig. 1D. By varying the delay, the THz

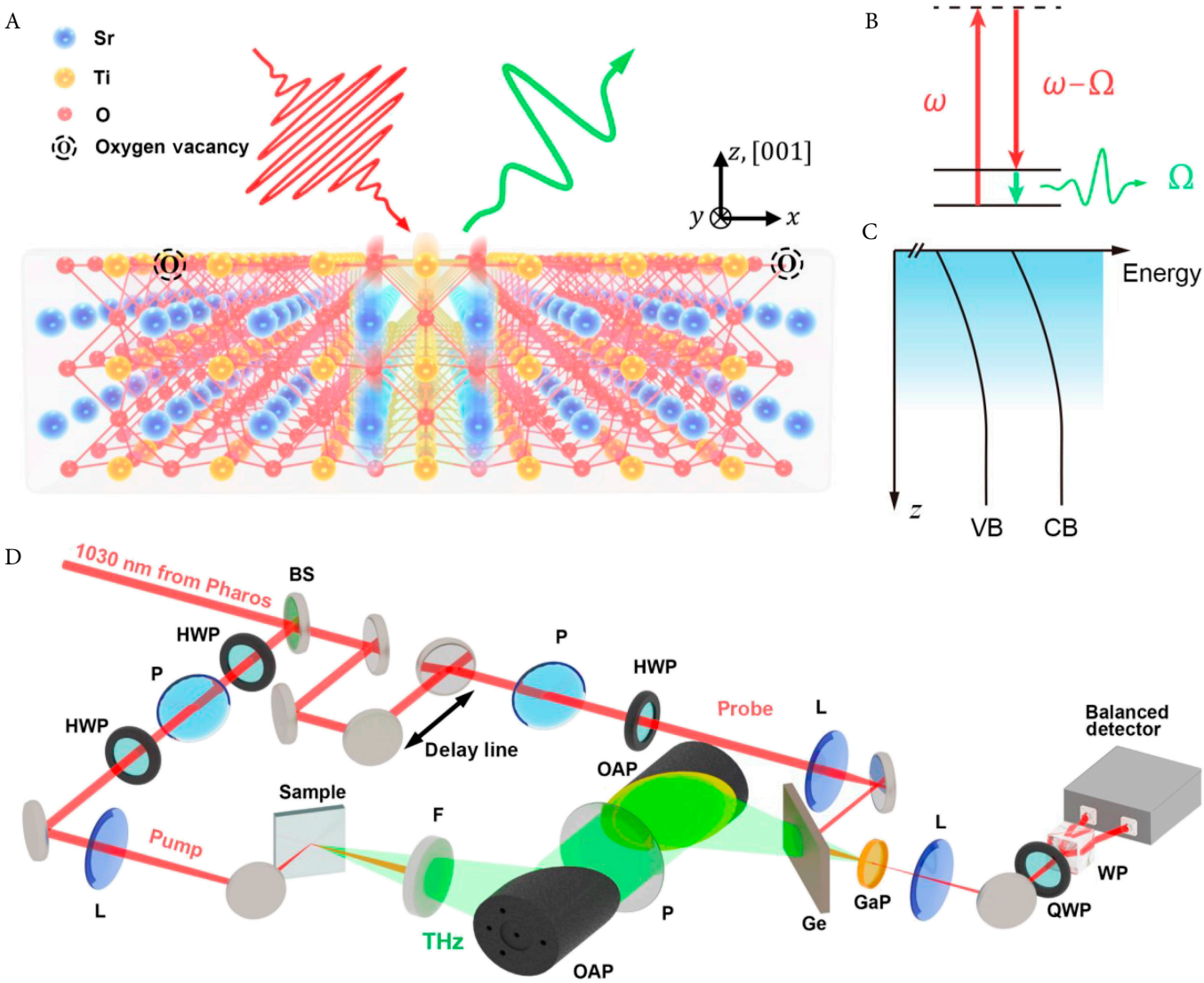

Fig. 1. Terahertz difference frequency spectroscopy. (A) Schematic of surface difference frequency generation from STO(001). (B) Energy level diagram of intra-pulse difference frequency generation. Ω, frequency component of THz output; ω, frequency component in the pump pulse. (C) Schematic of the band bending at the STO surface/interface. CB, conduction band; VB, valence band. (D) Sketch of the experimental setup. BS, beam splitter; HWP, half-wave plate; P, linear polarizer; L, lens; F, Teflon filter; OAP, off-angle parabolic mirror; QWP, quarter-wave plate; WP, Wollaston prism.

waveform in time domain was measured by recording the polarization change of the probe in EO crystal at different delay. The polarization change was measured using the balanced detection scheme consisting of a silicon photodiode-based balanced detector (Newport Nirvana) and a lock-in amplifier as shown in Fig. 1D. The measured THz waveform is transformed into frequency domain via fast Fourier transform (FFT) algorithm with time interval being 0.04 ps corresponding to the interval of time delay in EOS measurement. After the data processing procedure described in Section S3, the corresponding spectra of $\chi^{(2)}_{s,eff}$, including real and imaginary part, can be obtained.

Sensitivity of THz-DFS setup

The noise spectrum of our THz-DFS measurement setup with integration time over 100 s (10 million pulses) is shown in Fig. S6. Above 1.0 THz, the noise level is 2×10^{-22} m^2/V, which corresponds to 5×10^{-8} $rad/\sqrt{Hz}$ in our EOS measurement [26]. Below 1.0 THz, the sensitivity becomes worse toward the low frequency because of the loss by diffraction and the weaker radiation of the oscillating dipoles at lower frequencies. Notice that $\chi^{(2)}_{s,eff}$ of a self-assembled monolayer is in the order of 1×10^{-21} m^2/V. Thus, the sensitivity of our setup is sufficient for the detection of surface species with submonolayer thickness.

Results

To examine the validity of THz-DFS for probing the low-frequency resonances at surfaces and interfaces, STO interfaces with or without heterogeneous overlayers were chosen as the representatives. The DF process is not allowed in the centrosymmetric bulk of STO. At the interface, it is known that oxygen vacancies in the near-surface region of STO lead to band bending that breaks the centrosymmetry in the interfacial

region (Fig. 1C). Therefore, the DFS spectrum must consist of contributions from the true surface layer and the surface electric field-induced polarization in the band-bending region, corresponding to $\chi_s^{(2)}$ and $\chi_B^{(3)} \int E_0(z)e^{i\Delta kz}dz$ in Eq. 2, respectively [28]. Through symmetry analysis on the TO1 phonon polarized in the band bending region, one can show that the second term in Eq. 2 is allowed in *ppp*-polarization combination (*p*-polarized THz emission and *p*-polarized pump fields, $\chi^{(3)}_{B,zzzz} \neq 0$) but vanishes in *pss* (*p*-polarized THz emission and *s*-polarized pump fields, $\chi^{(3)}_{B,zzyy} = 0$) (see Section S3). The true surface term, on the other hand, exists in *pss* ($\chi^{(2)}_{s,zyy} \neq 0$). Thus, through proper selection of polarization combination, one can probe the two contributions separately.

It is well known that the two-dimensional electron gas (2DEG) emerges at the interfaces of Al_2O_3/STO or $LaAlO_3$/$SrTiO_3$ (LAO/STO) when the overlayer reaches critical thickness [29,30], but is absent for bare STO surface, SiO_2/STO, or thin LAO/STO interfaces. The DFS signal from 2DEG is nonvanishing under *pss*-polarization (see Section S3). The DFS waveform from the 20-nm Al_2O_3/STO interface is presented in Fig. 2A measured under *pss*-polarization at room temperature. The linear dependence of THz amplitude on pump intensity confirms the signal resulting from the second-order nonlinear process (see Section S1 and Fig. S1). After Fourier transform and normalization against a reference quartz, we display the resultant imaginary parts of the DFS spectrum in Fig. 2B. The imaginary spectrum, $\mathrm{Im}\chi^{(2)}_{s,eff}$, is more informative as it explicitly characterizes the surface/interface resonances. Figure 2B and D presents the imaginary spectra from various STO interfaces. The Drude-like behavior of 2DEG diverging toward the low frequencies is clearly observed in the DFS spectra for 20-nm Al_2O_3/STO and 6-unit-cell LAO/STO. In contrast, the DFS spectra of 2-unit-cell LAO/STO, 50-nm SiO_2/STO, and air/STO interfaces essentially show no signal in the spectral range of 1 to 4 THz, signifying that no 2DEG exists at these interfaces [29]. The DFS spectra for the interfaces of 20-nm Al_2O_3/STO and 6-unit-cell LAO/STO can be nicely fitted using the hydrodynamic model of free carriers [31]. It is worthwhile to mention that, although 2DEG can also be characterized using linear reflection spectroscopy, the measured spectrum

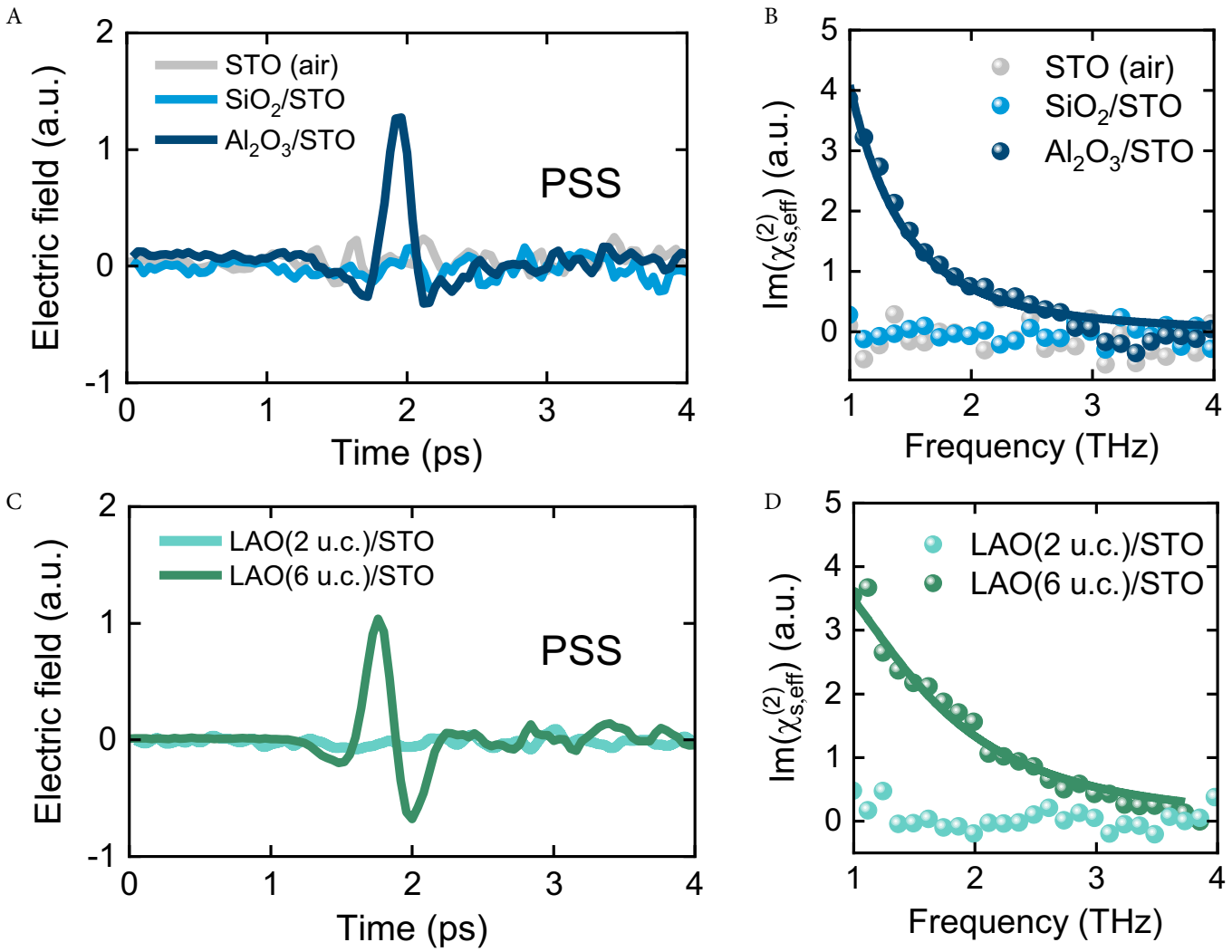

Fig. 2. THz-DFS of 2DEG at STO interfaces. (A) THz waveform from bare STO(001) (gray), 20-nm-thick Al_2O_3/STO(001) (dark blue), and 50-nm-thick SiO_2/STO(001) (blue) under *pss*-polarization combination. (B) Spectra of $\mathrm{Im}\chi^{(2)}_{s,eff}$ corresponding to (A). (C) THz waveform from 2-unit-cell (u.c.) LAO/STO(001) (light green) and 6-unit-cell LAO/STO(001) (dark green). (D) Corresponding $Im\,\chi^{(2)}_{s,eff}$ spectra to (C). Dark blue curve in (B) and dark green curve in (D) serve as eye guide.

consists of a huge background from the bulk [32], causing difficulties in deducing the 2DEG spectrum unambiguously. Moreover, the contributions from 2DEG at the interface and the doping carriers deeper in the bulk are hardly separable in the linear spectroscopy. In contrast, the THz-DFS is capable of characterizing 2DEG and other species at the surface/interface that naturally eliminates the bulk background.

Surface/interface potential is not only critically important for the electronic properties at the interface, including the emergence of 2DEG, but is the essential factor for electron-hole separation and charge transfer across the interface in chemistry. In STO, the surface oxygen vacancy or charge transfer at the heterogeneous interface causes band bending in the interfacial region [33–35]. Accordingly, the lattice structure of STO is polarized by the electric field in the band bending region. The broken centrosymmetry of STO in the interfacial region can be measured by DFS by monitoring the polarized phonon that is directly related to the surface/interface potential, Φ. Thus, once the $\chi^{(3)}_B$ spectrum of STO is calibrated in prior (described in Section S5 and Figs. S4 and S5), Φ can be determined in situ using THz-DFS following Eq. 2 or 3.

Figure 3A and B displays the DFS waveform, amplitude, imaginary, and real spectra of bare STO in dry air under *ppp*-polarization combination. A single resonant peak is recognized at 2.8 THz with 0.7-THz bandwidth (full width at half maximum, FWHM) in the DF spectrum, which can be readily assigned to the TO1 phonon of STO [36]. As compared in Fig. 3C, the DF spectrum of bare STO surface shares the same resonant frequency and linewidth with the linear absorption spectrum of the TO1 phonon in bulk STO [36]. Note that the effective thickness of the band-bending region is ~100 nm for a pristine STO, which is two orders of magnitude greater than that of a typical surface layer. Thus, the *ppp*-DF spectrum of STO is dominated by surface electric field-induced polarization over the pure surface contribution. As compared also in Fig. 3C, the *ppp*-DF spectra of Al_2O_3/STO and bare STO exhibit the same resonant features, except for the amplitude of the TO1 mode due to the difference in interface potential (see Eq. 3).

Figure 4A compares a set of *ppp*-DFS spectra of air/STO, SiO_2/STO, Al_2O_3/STO, and LAO/STO interfaces. It is noteworthy that the center frequency and bandwidth of all $\mathrm{Im}\chi^{(2)}_{s,eff}$ spectra in Fig. 4A are the same. The absence of extra spectral mode evidently shows the $\chi^{(3)}_B$ contribution from band bending region dominated the measured spectra [37]. The corresponding surface/interface potential deduced using Eq. 2 or 3 is plotted in Fig. 4B. The interface potential of STO with 20-nm-thick Al_2O_3 overlayer was found to be +0.58 V, which agrees with that determined by x-ray photo-emission spectroscopy (XPS) [38]. It confirms the validity of our optical technique for the measurement of surface/interface potential. In Fig. 4B, we see no clear correlation between surface/interface potential and the emergence of 2DEG. In particular, the *ppp*-DF spectra for 6-unit-cell LAO/STO and 2-unit-cell LAO/STO are essentially the same (see inset of Fig. 4A), indicating the same interface potential of +0.45 V, although the former hosts 2DEG at the interface. It suggests that increasing LAO thickness does not

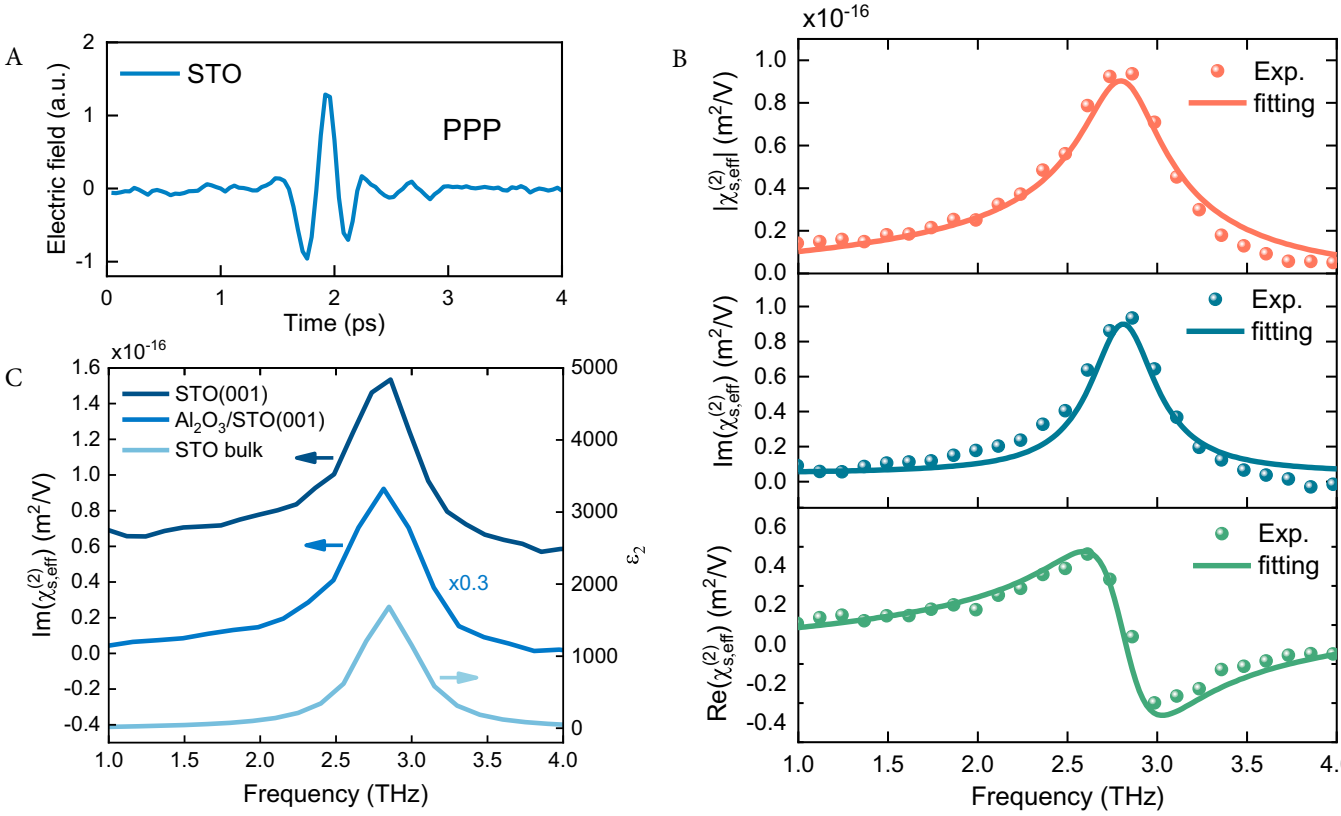

Fig. 3. THz difference frequency spectrum of $SrTiO_3$. (A) Typical waveform of the emitted THz pulse from STO(001). (B) Amplitude, real part and imaginary part of deduced surface second-order susceptibility, after normalization against z-cut quartz reference and removal of Fresnel factor. (C) Comparison between bare STO(001) (top), Al_2O_3/STO(001) (middle), and the imaginary part of dielectric function (ε_2) of bulk STO (bottom) [36].

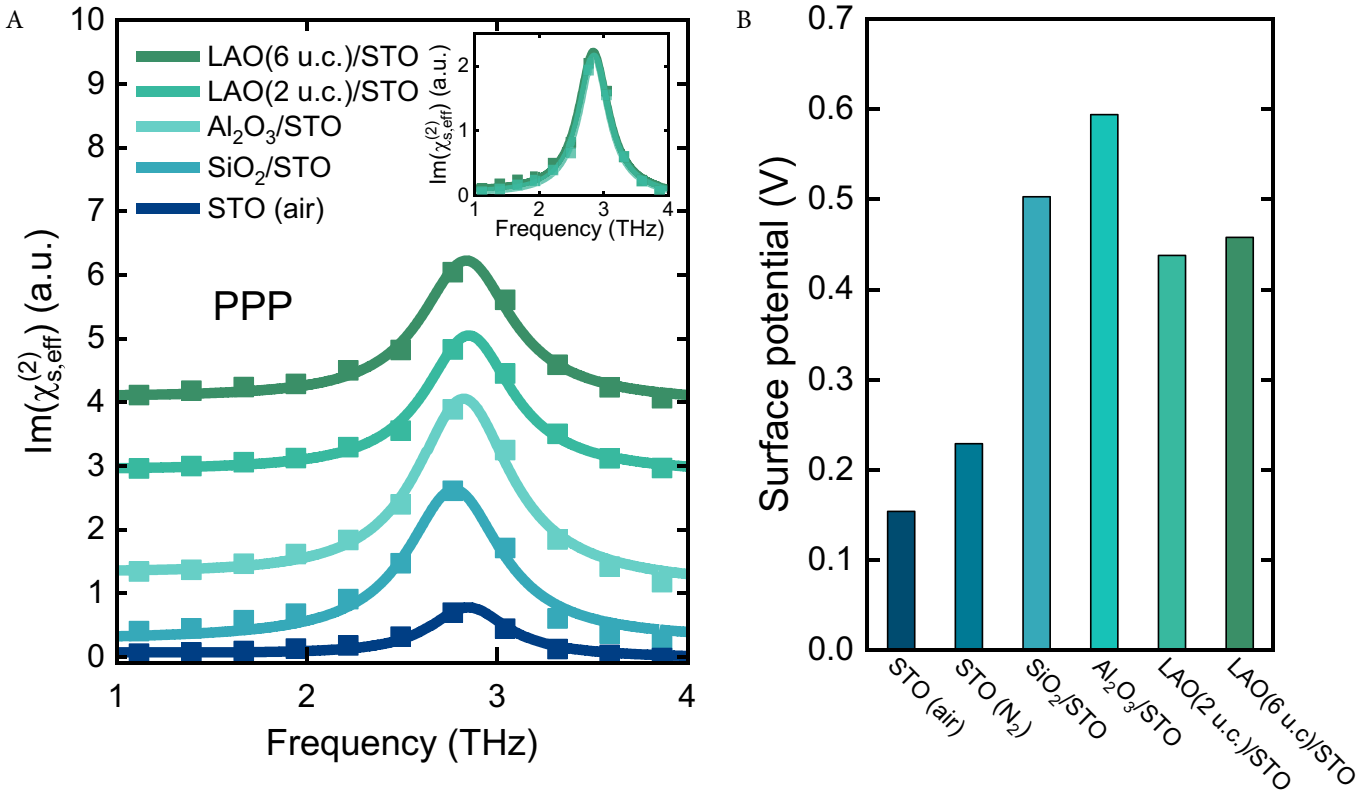

Fig. 4. Surface potential of STO measured by THz-DFS. (A) Spectra of $\mathrm{Im}\chi^{(2)}_{s,eff}$ under *ppp*-polarization combination, stacked from bottom to top for bare STO, SiO_2/STO, Al_2O_3/STO, 2-unit-cell LAO/STO, and 6-unit-cell LAO/STO. Inset: Comparison between the spectra of 2-unit-cell LAO/STO and 6-unit-cell LAO/STO. (B) Summary chart of surface/interface potential of STO(001) in various conditions.

cause an obvious change in the interface potential but may lead to the formation of a dipole layer across the interface that creates a potential well at the topmost layers of STO for the confinement of 2DEG [39]. These results demonstrate THz-DFS as a feasible tool to quantify the surface/interface potential, with unique advantages including chemical selectivity through resonances, functionality for buried interfaces, and remote monitoring.

Discussion

Our work established THz-DFS as a viable surface-specific nonlinear optical spectroscopic method for probing low-frequency resonances on the surface or at the buried interface. As a demonstration, STO(001) surface and interfaces with different heterogeneous overlayers were investigated. The resonant features of interfacial species and the surface/interface potential were characterized with THz-DFS. The sensitivity of THz-DFS also satisfies the detection requirement of submonolayer surface species in general using the state-of-the-art EOS technique. In contrast, the well-established SFS found successful applications in probing the elementary vibrations in the mid-IR region, e.g., the chemical and biological materials composed of light atoms. Our approach opens up new opportunities for exploring low-frequency vibrations and emergent species on surfaces or at buried interfaces in various environments.

As an outlook, the detection bandwidth of THz-DFS that we demonstrated here is limited by the EO crystal. Using a high-quality organic EO crystal, the detection bandwidth can reach beyond 5 THz. Research in this frequency range is intriguing because collective excitations at the interface of various condensed matter systems occur between 5 and 15 THz, such as superconducting gap, heavy Fermion plasmons, and soft mode in ferroelectricity.

Acknowledgments

We thank Y. Ron Shen (University of California, Berkeley) for the fruitful discussion and R. Peng and T. Zhang (Fudan University) for supplying samples. **Funding:** C.T. acknowledges the funding support from the National Key Research and Development Program of China (nos. 2021YFA1400503 and 2021YFA1400202), the National Natural Science Foundation of China (nos. 12125403, 11874123, and 12221004), and the Shanghai Science and Technology Committee (no. 20ZR1406000). L.C. acknowledges the support from the National Natural Science Foundation of China (no. 12104305). X.Z. acknowledges the support from the Science and Technology Commission of Shanghai Municipality (no. 21JC1405000). **Competing interests:** The authors declare that they have no competing interests.

Data Availability

All data needed to evaluate the conclusions in the paper are present in the paper and/or the Supplementary Materials.

Supplementary Materials

Supplementary Text
Figs. S1 to S7

References

1. Zubko P, Gariglio S, Gabay M, Ghosez P, Triscone JM. Interface physics in complex oxide Heterostructures. *Annu Rev Condens Matter Phys*. 2011;2(2):141–165.
2. Hwang HY, Iwasa Y, Kawasaki M, Keimer B, Nagaosa N, Tokura Y. Emergent phenomena at oxide interfaces. *Nat Mater*. 2012;11(2):103–113.
3. Pai YY, Tylan-Tyler A, Irvin P, Levy J. Physics of SrTiO3-based heterostructures and nanostructures: A review. *Rep Prog Phys*. 2018;81(3):036503.
4. Yadav AK, Nelson CT, Hsu SL, Hong Z, Clarkson JD, Schlepuetz CM, Damodaran AR, Shafer P, Arenholz E, Dedon LR, et al. Observation of polar vortices in oxide superlattices. *Nature*. 2016;530(7589):198–201.
5. Wang QY, Li Z, Zhang WH, Zhang ZC, Zhang JS, Li W, Ding H, Ou YB, Deng P, Chang K, et al. Interface-induced high-temperature superconductivity in single unit-cell FeSe films on SrTiO3. *Chin Phys Lett*. 2012;29(3):037402.
6. Zhang HM, Zhang D, Lu XW, Liu C, Zhou GY, Ma XC, Wang LL, Jiang P, Xue QK, Bao XH. Origin of charge transfer and enhanced electron-phonon coupling in single unit-cell FeSe films on SrTiO3. *Nat Commun*. 2017;8:214.
7. Lee JJ, Schmitt FT, Moore RG, Johnston S, Cui YT, Li W, Yi M, Liu ZK, Hashimoto M, Zhang Y, et al. Interfacial mode coupling as the origin of the enhancement of T-c in FeSe films on SrTiO3. *Nature*. 2014;515(7526):245–248.
8. Li Q, Stoica VA, Paściak M, Zhu Y, Yuan Y, Yang T, McCarter MR, Das S, Yadav AK, Park S, et al. Subterahertz collective dynamics of polar vortices. *Nature*. 2021;592(7854):376–380.
9. Takata T, Jiang J, Sakata Y, Nakabayashi M, Shibata N, Nandal V, Seki K, Hisatomi T, Domen K. Photocatalytic water splitting with a quantum efficiency of almost unity. *Nature*. 2020;581(7809):411–414.
10. Wrighton MS, Ellis AB, Wolczanski PT, Morse DL, Abrahamson HB, Ginley DS. Strontium titanate photoelectrodes. Efficient photoassisted electrolysis of water at zero applied potential. *J Am Chem Soc*. 1976;98(10):2774–2779.
11. Wagner F, Somorjai G. Photocatalytic hydrogen production from water on Pt-free SrTiO 3 in alkali hydroxide solutions. *Nature*. 1980;285(5766):559–560.
12. Shen YR. *Fundamentals of sum-frequency spectroscopy*. Cambridge (UK): Cambridge University Press; 2016.
13. Dhillon SS, Vitiello MS, Linfield EH, Davies AG, Hoffmann MC, Booske J, Paoloni C, Gensch M, Weightman P, Williams GP, et al. The 2017 terahertz science and technology roadmap. *J Phys D Appl Phys*. 2017;50(4):043001.
14. Salén P, Basini M, Bonetti S, Hebling J, Krasilnikov M, Nikitin AY, Shamuilov G, Tibai Z, Zhaunerchyk V, Goryashko V. Matter manipulation with extreme terahertz light: Progress in the enabling THz technology. *Phys Rep*. 2019;836-837:1–74.
15. Pluchery O, Humbert C, Valamanesh M, Lacaze E, Busson B. Enhanced detection of thiophenol adsorbed on gold nanoparticles by SFG and DFG nonlinear optical spectroscopy. *Phys Chem Chem Phys*. 2009;11(35):7729–7737.
16. Tadjeddine A. Spectroscopic investigation of surfaces and interfaces by using infrared-visible sum and difference frequency generation. *Surf Rev Lett*. 2000;07(04):423–436.
17. Kadlec F, Kuzel P, Coutaz JL. Optical rectification at metal surfaces. *Opt Lett*. 2004;29(22):2674–2676.
18. Zhang XC, Hu BB, Darrow JT, Auston DH. Generation of femtosecond electromagnetic pulses from semiconductor surfaces. *Appl Phys Lett*. 1990;56(11):1011–1013.
19. Maysonnave J, Huppert S, Wang F, Maero S, Berger C, de Heer W, Norris TB, De Vaulchier LA, Dhillon S, Tignon J, et al. Terahertz generation by dynamical photon drag effect in graphene excited by femtosecond optical pulses. *Nano Lett*. 2014;14(10):5797–5802.
20. Huang Y, Yao Z, He C, Zhu L, Zhang L, Bai J, Xu X. Terahertz surface and interface emission spectroscopy for advanced materials. *J Phys Condens Matter*. 2019;31(15):153001.
21. Perets EA, Yan EC. Chiral water superstructures around antiparallel β-sheets observed by chiral vibrational sum frequency generation spectroscopy. *J Phys Chem Lett*. 2019;10(12):3395–3401.
22. Choi WJ, Yano K, Cha M, Colombari FM, Kim J-Y, Wang Y, Lee SH, Sun K, Kruger JM, de Moura AF, et al. Chiral phonons in microcrystals and nanofibrils of biomolecules. *Nat Photonics*. 2022;16:366–373.
23. Wen YC, Zha S, Liu X, Yang SS, Guo P, Shi GS, Fang HP, Shen YR, Tian CS. Unveiling microscopic structures of charged water interfaces by surface-specific vibrational spectroscopy. *Phys Rev Lett*. 2016;116(1):016101.
24. Ohno PE, Saslow SA, Wang H-J, Geiger FM, Eisenthal KB. Phase-referenced nonlinear spectroscopy of the α-quartz/water interface. *Nat Commun*. 2016;7(1):13587.
25. Ong S, Zhao X, Eisenthal KB. Polarization of water molecules at a charged interface: Second harmonic studies of the silica/water interface. *Chem Phys Lett*. 1992;191(3):327–335.
26. Wang YH, Ma JY, Le JM, Su YD, Tian CS. Enhanced sensitivity of terahertz electro-optic sampling based on reflective Brewster window. In Press.
27. Zhang S, Fu ZY, Zhu BB, Fan GY, Chen YD, Wang SJ, Liu YX, Baltuska A, Jin C, Tian CS, et al. Solitary beam propagation in periodic layered Kerr media enables high-efficiency pulse compression and mode self-cleaning. *Light Sci Appl*. 2021;10(1):53.
28. Meirzadeh E, Christensen DV, Makagon E, Cohen H, Rosenhek-Goldian I, Morales EH, Bhowmik A, Lastra JMG, Rappe AM, Ehre D, et al. Surface pyroelectricity in cubic SrTiO3. *Adv Mater*. 2019;31(44):e1904733.
29. Berner G, Müller A, Pfaff F, Walde J, Richter C, Mannhart J, Thiess S, Gloskovskii A, Drube W, Sing M, et al. Band alignment in LaAlO3/SrTiO3 oxide heterostructures inferred from hard x-ray photoelectron spectroscopy. *Phys Rev B*. 2013;88(11):115111.
30. Chen YZ, Bovet N, Trier F, Christensen DV, Qu FM, Andersen NH, Kasama T, Zhang W, Giraud R, Dufouleur J, et al. A high-mobility two-dimensional electron gas at the spinel/perovskite interface of γ-Al2O3/SrTiO3. *Nat Commun*. 2013;4(1):1371.
31. Kravtsov V, AlMutairi S, Ulbricht R, Kutayiah AR, Belyanin A, Raschke MB. Enhanced third-order optical nonlinearity driven by surface-Plasmon field gradients. *Phys Rev Lett*. 2018;120(20):203903.
32. Dubroka A, Rössle M, Kim KW, Malik VK, Schultz L, Thiel S, Schneider CW, Mannhart J, Herranz G, Copie O, et al. Dynamical response and confinement of the electrons at the LaAlO3/SrTiO3 Interface. *Phys Rev Lett*. 2010;104(15):156807.
33. Bickel N, Schmidt G, Heinz K, Muller K. Ferroelectric relaxation of the Srtio3(100) surface. *Phys Rev Lett*. 1989;62(17):2009–2011.

34. Noguera C. Polar oxide surfaces. *J Phys Condens Mat*. 2000;12(31):R367–R410.
35. Zhang Z, Yates JT. Band bending in semiconductors: Chemical and physical consequences at surfaces and interfaces. *Chem Rev*. 2012;112(10):5520–5551.
36. Dore P, DeMarzi G, Paolone A. Refractive indices of SrTiO3 in the infrared region. *Int J Infrared Milli*. 1997;18(1): 125–138.
37. Benjamin R, Emily M, Shyam P, Emma LD, Tianli L, Franz MG, Julianne MG. Water structure in the electrical double layer and the contributions to the total interfacial potential at different surface charge densities. *J Am Chem Soc*. 2022;144(36): 16338–16349.
38. Schütz P, Pfaff F, Scheiderer P, Chen YZ, Pryds N, Gorgoi M, Sing M, Claessen R. Band bending and alignment at the spinel/perovskite γ-Al2O3/SrTiO3 heterointerface. *Phys Rev B*. 2015;91(16):165118.
39. Yu L, Zunger A. A polarity-induced defect mechanism for conductivity and magnetism at polar–nonpolar oxide interfaces. *Nat Commun*. 2014;5(1):5118.